Title
MR imaging of the normal shoulder: anatomic correlation.

Journal
American Journal of Roentgenology, 148(1)

ISSN
0361-803X

Authors
Seeger, LL
Ruszkowski, JT
Bassett, LW
et al.

Publication Date
1987

DOI
10.2214/ajr.148.1.83

Peer reviewed

MR Imaging of the Normal Shoulder: Anatomic Correlation

Leanne L. Seeger[1]
June T. Ruszkowski[2]
Lawrence W. Bassett[1]
Stephen P. Kay[3, 4]
Richard D. Kahmann[3]
Harvard Ellman[5]

The complex anatomy and the requirement to image in the peripheral magnetic field have made the shoulder difficult to examine with MR. However, the use of high-resolution scanning techniques and specialized surface coils has improved the quality of MR images obtained. Seventy-five scans of the shoulders of normal volunteers were correlated with multiplanar cryomicrosections of six cadaver shoulders to study the MR appearance of normal structures. MR was shown to provide excellent depiction of shoulder anatomy.

MR is a useful tool for imaging the musculoskeletal system. Exquisite depiction of the bone marrow rivals or surpasses other imaging techniques [1, 2]. Soft tissues are clearly delineated because normal fat, muscle, hyaline cartilage, and fibrous tissue have different individual signal intensities [3, 4]. Radiation exposure is avoided and arthrography may be unnecessary.

However, the shoulder poses several unique difficulties for imaging with MR. Because of space limitations in the magnet, the shoulder cannot be positioned in the center of the magnetic field. This necessitates shifting laterally for image centering and scanning in a region where the signal-to-noise ratio is low. Also, because diseases of the shoulder usually involve small soft-tissue structures, high-resolution scans are needed to provide diagnostic information. This requires steep magnetic gradients, which decrease the MR signal. These problems can be overcome by combining high-resolution scanning with the use of a surface coil [5, 6]. Finally, the bony and soft tissues of the shoulder are oriented along multiple nonorthogonal axes, necessitating oblique scanning [7, 8].

The goal of this study is to determine if MR allows detailed evaluation of the anatomic structures comprising the normal shoulder joint and to correlate the MR images with cadaver cryomicrosections.

Materials and Methods

Scan and Cryomicrosection Planes

The MR images and anatomic sections were made in the orthogonal planes and a frontal oblique plane along the course of the supraspinatus muscle. The oblique axis was required to visualize both the continuity of the supraspinatus muscle-tendon unit and the relationship of this tendon to the acromion and acromioclavicular joint above.

Scanning Technique

Seventy-five scans of 20 shoulders were obtained in healthy young adults. Scanning was performed on a Fonar Beta-3000 0.3-T permanent-magnet imaging system by using a spin-echo pulse sequence with TR = 500 msec, TE = 28 msec. A 256 × 256 imaging matrix was used and was interpolated to 512 × 512 for display. Pixel size was 0.75 mm^2. Slice thickness was 5 mm, obtained at 7-mm intervals. With four excitations, scan time was 8.33 min for a

Received February 7, 1986; accepted after revision August 20, 1986.

Presented at the annual meeting of the American Roentgen Ray Society, Washington, DC, April 1986.

Recipient of the 1986 ARRS President's Resident Award.

This work was supported in part by a grant from the James T. Case Foundation, UCLA Department of Radiological Sciences.

[1] Department of Radiological Sciences, UCLA School of Medicine, Los Angeles, CA 90024. Address reprint requests to L. L. Seeger.

[2] 30-64 34th St., Astoria, NY 11103.

[3] Department of Surgery, Division of Orthopedic Surgery, UCLA School of Medicine, Los Angeles, CA 90024.

[4] Present address: Department of Orthopedic Surgery, University of Texas Medical School, San Antonio, TX 78284.

[5] 2080 Century Park E., Ste. 1500, Los Angeles, CA 90067.

AJR **148:83-91, January 1987**
0361-803X/87/1481-0083

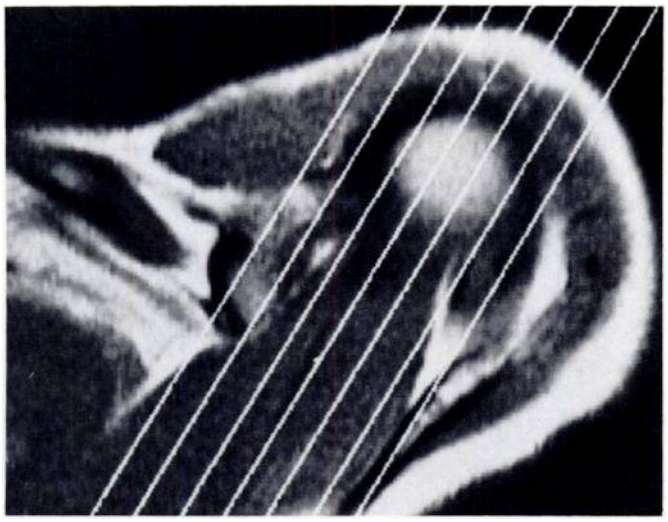

Fig. 1.—Axial scout scan showing cursor alignment through the long axis of the supraspinatus belly for oblique imaging.

multislice series of seven images. The amount of lateral shift required for image centering depended on patient size, varying from 80 to 120 mm from center toward the shoulder to be scanned. This was accomplished by manipulation of the radiofrequency to allow the imaging plane to be moved in any desired direction.

An 18-cm or 22.5-cm diameter planar surface coil was used, with the size determined by the body build of the subject. The coil was positioned obliquely over the shoulder such that its axis was perpendicular to the magnetic field. Foam wedges placed between the inner surface of the coil and the patient assisted in maintaining coil alignment and allowed for signal uniformity over the entire area to be imaged.

A standard position was chosen to provide consistency in anatomic relationships while maximizing comfort. The arm was placed across the abdomen (therefore internally rotated), and the elbow was elevated to parallel the humeral head.

An axial scan was used as a scout for the frontal oblique plane, which allowed precise sagittal-to-coronal alignment along the long axis of the supraspinatus belly (Fig. 1).

A

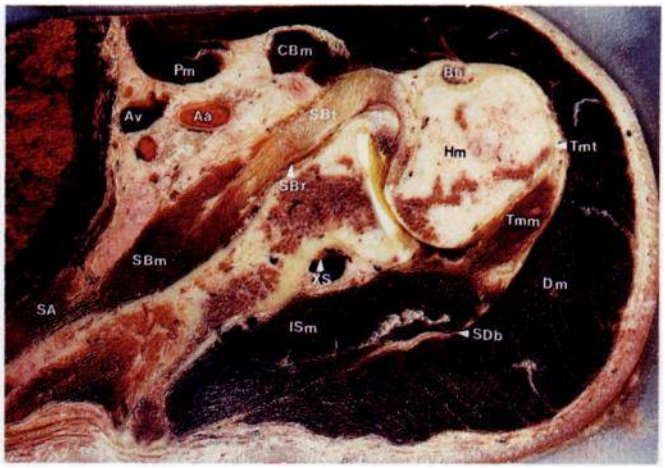

B

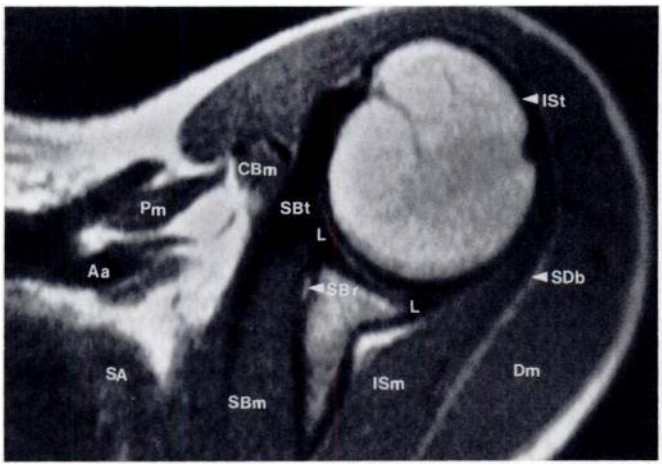

C

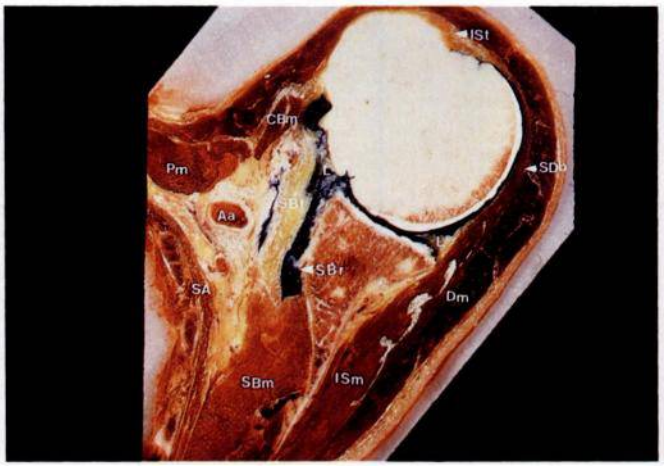

D

Fig. 2.—*A–H*, MR images and photographs of cadaver specimens made in the axial plane. Serial images from inferior to superior are shown. See Key to Abbreviations on page 86.

Cadaver Preparation and Sectioning

Six fresh cadaver shoulders were used for anatomic study. Available cadavers were elderly and had degenerative changes. Specimens with major shoulder abnormalities were excluded after evaluation with fluoroscopy and, when necessary, limited arthrography. Aortic injection of plaster mixed with red dye forced deoxygenated blood into the venous system. Blue dye mixed with dilute radiographic contrast material was injected under fluoroscopic control into two shoulders to define the joint space. Care was taken to avoid excessive joint distension that would distort anatomic relationships.

After injection, the cadavers were frozen with the lower arm across the abdomen, causing internal rotation of the shoulder similar to the position used for scanning. The shoulders were then block resected, cryomicrosectioned (LKB 2250, Bromma, Sweden), and photographed at 0.5-mm intervals [9]. One shoulder was sectioned in each of the axial, coronal, sagittal, and frontal oblique planes. Because of the superior depiction of several structures in the axial and oblique projections, sectioning in these two planes was repeated on the shoulders that had been injected with blue intraarticular dye.

Results

Although the plane of optimal visualization varied, MR depicted the humeral head, acromion, distal clavicle, acromioclavicular joint, hyaline cartilage of the glenohumeral joint, glenoid labrum, rotator cuff muscles and tendons, joint capsule, and the coracoclavicular ligament. Identification of nerves and vascular structures was enhanced either by surrounding fat or flow through the vessels.

With this T1-weighted sequence, the MR appearance of the osseous structures is as expected: cortical bone has no signal, and a bright signal originates form the marrow cavity. The humeral head epiphysis can be differentiated from the

E

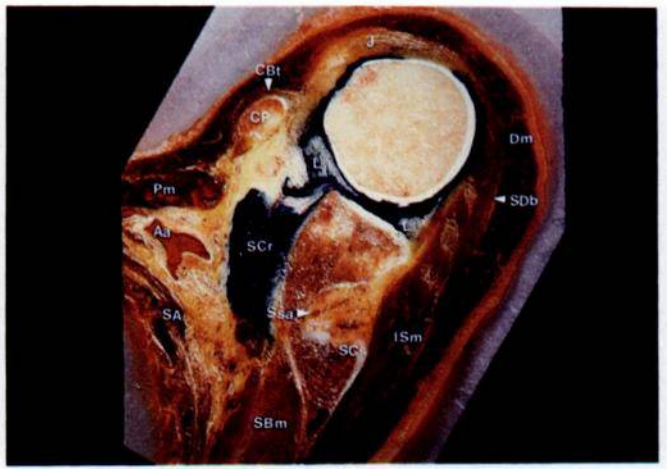

F

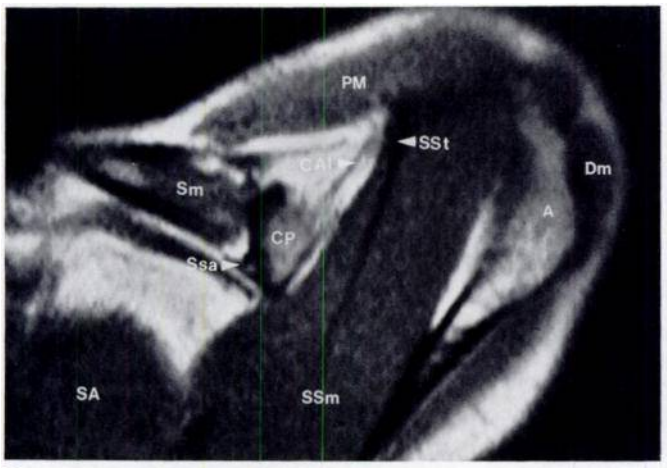

G

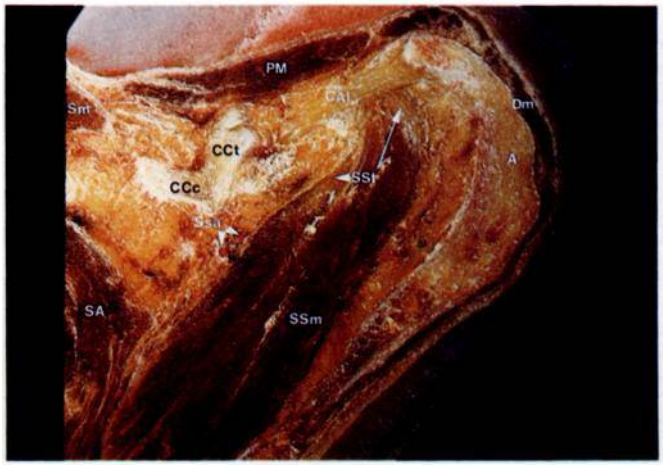

H

metaphysis in normal young adults because the epiphyseal signal is brighter. Ligaments and tendons have a very low signal intensity, which allows differentiation from the adjacent brighter muscle. Precise sites of bony attachment cannot be seen because of the similar signal-void associated with cortical bone. Likewise, the low signal intensity of the fibrous joint capsule cannot be differentiated from the glenohumeral ligaments or the cuff tendons that lie adjacent to and are incorporated into the capsule [10–12]. The glenoid labrum is a redundant fold of the joint capsule [10]; accordingly, this structure appears homogeneously black, typical of fibrous tissue. The signal of the articular hyaline cartilage of the humeral head and glenoid is bright, which contrasts well against the low-signal cortical bone and labrum. The two surfaces of hyaline cartilage cannot be seen as separate at the site of coaptation. The subacromial-subdeltoid bursa is not distended with fluid in the normal state [11, 13]. This flat but expansive potential space is represented by a thin band of high signal intensity, corresponding to abundant fat both within and beneath the synovial lining [10, 11, 14].

Key to Abbreviations Used in Figures

A	acromion
Aa	axillary artery
ACj	acromioclavicular joint
AHl	acromiohumeral ligament
Ar	axillary recess
Av	axillary vein
Ba	brachial artery
BG	bicipital groove
Bm	biceps (long head) muscle
Bt	biceps (long head) tendon
C	clavicle
CAl	coracoacromial ligament
CBm	coracobrachialis/biceps (short head) muscle
CBt	coracobrachialis/biceps (short head) tendon
CCc	coracoclavicular ligament, conoid
CCt	coracoclavicular ligament, trapezoid
CHl	coracohumeral ligament
CP	coracoid process
Cv	cephalic vein
Dm	deltoid muscle
Dt	deltoid tendon
He	humeral head epiphysis
HC	hyaline cartilage
Hm	humeral head metaphysis
ISm	infraspinatus muscle
ISt	infraspinatus tendon
J	joint capsule
L	glenoid labrum
PM	pectoralis major muscle
Pm	pectoralis minor muscle
SA	serratus anterior muscle
Sba	subscapular artery and branches
SBm	subscapularis muscle
SBr	subscapularis recess
SBt	subscapularis tendon
SCb	scapula body
SCr	subcoracoid recess
SCs	scapula spine
SCu	scapula upper (superomedial) aspect
SDb	subdeltoid bursa
Sm	subclavis muscle
Ssa	suprascapular artery and branches
SSm	supraspinatus muscle
SSt	supraspinatus tendon
Tm	trapezius muscle
TLm	triceps (long head) muscle
TLt	triceps (long head) tendon
TM	teres major muscle
Tmm	teres minor muscle
Tmt	teres minor tendon
XA	anterior circumflex humeral artery
XP	posterior circumflex humeral artery
XS	circumflex scapular artery and branches

Axial scans (Fig. 2) clearly show the anteroposterior alignment of the glenohumeral articulation. The inferior humeral head is oblong, and the posterolateral aspect is noticeably flat. Continuous with this surface is an indentation on the posterolateral aspect of the midhumeral head. Both of these regions lack hyaline cartilage and serve as sites of attachment for some fibers of the teres minor and infraspinatus tendons. The head becomes progressively rounder superiorly. Marrow within the humeral head is inhomogeneous because of the oblique anterior-to-posterior axis of the physis. This appearance is especially evident at the level of the mid-head but may extend quite far superiorly. Axial scans provide good depiction of the low-signal glenoid labrum. The shape of this structure is significantly influenced by the position of the humeral head [10]. With internal rotation, the anterior labrum is larger than the posterior at all levels, and its apex is pointed. The contour of the posterior labrum is smooth throughout. A thin rim of medium to high signal intensity allows the labrum to be seen as separate from the adjacent capsule and cuff tendons. This corresponds to synovial folds that extend into the joint cavity [11, 14, 15]. As with the labrum, the appearance of these folds is influenced by humeral-head rotation [10, 14, 15]. The bicipital groove can be readily identified; however, the tendon within it cannot be distinguished from surrounding cortical bone or the transverse humeral ligament. A small region of bright signal is occasionally seen within the intertubercular sulcus, either adjacent to or surrounding the biceps tendon. The tendons of the subscapularis, infraspinatus, and teres minor muscles are visible over their entire lengths. The variable development of the three glenohumeral ligaments is indirectly evident by the extent of the subscapularis recess [10, 12].

In the coronal plane (Fig. 3), the coracoclavicular ligament, acromioclavicular joint, and superior humeral-head articular cartilage are well seen. The transition from supraspinatus muscle to tendon is gradual [12]. Because the coronal plane traverses this junction obliquely, inhomogeneous medium signal intensity is seen above the humeral head, and the expected signal-void of the tendon is only evident at its most lateral extent.

In the sagittal plane (Fig. 4), the oblique alignment of the physis is easily identified, and possible confusion arising from the inhomogeneity on axial scans is avoided. This plane also reveals the horizontal axis of the acromion and its relationship to the supraspinatus tendon.

The oblique plane (Fig. 5) shows the supraspinatus muscle and tendon in continuity. The relationship of the inferior acromion and acromioclavicular joint to the supraspinatus ten-

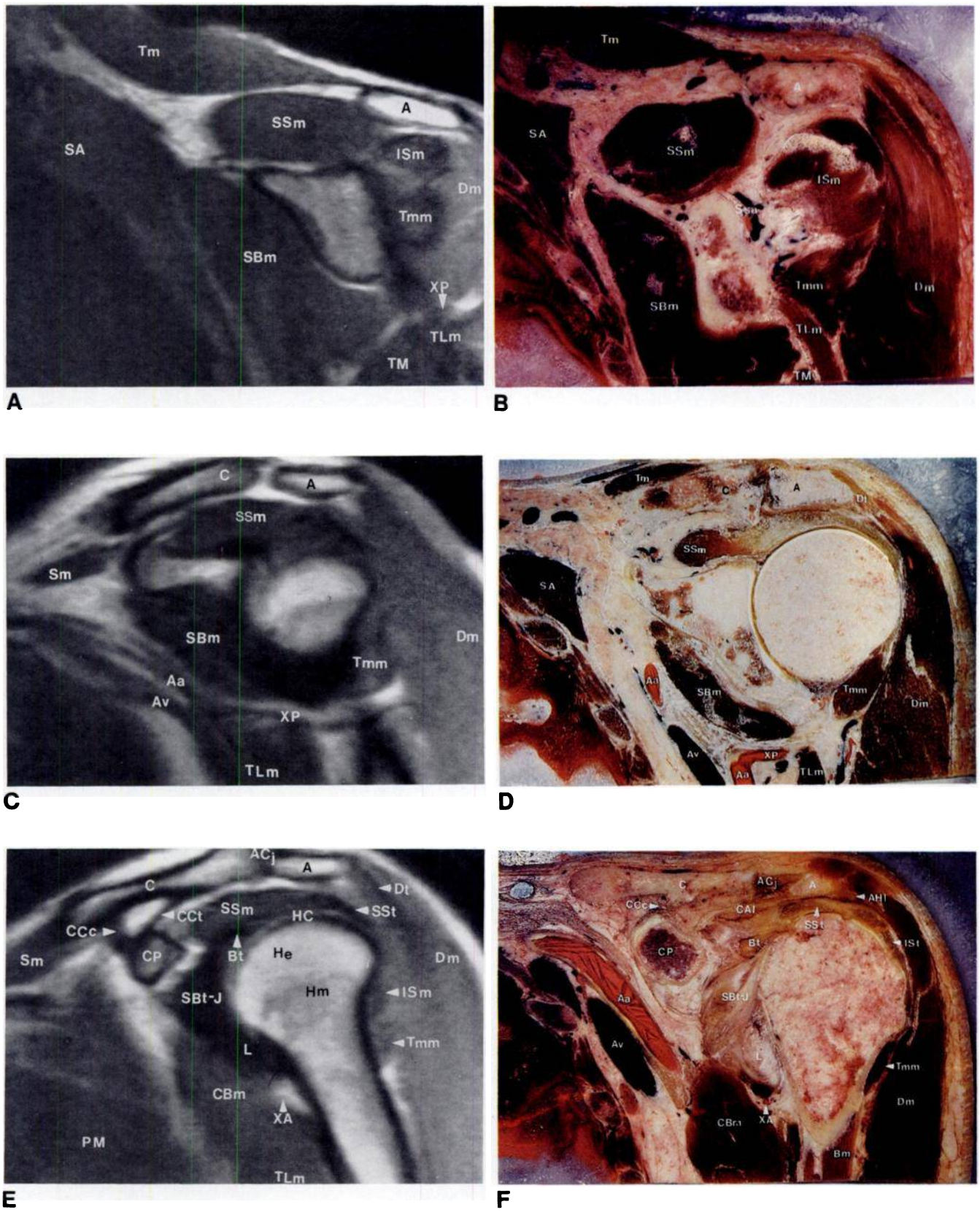

Fig. 3.—*A–F*, MR images and photographs of cadaver specimens made in the coronal plane. Serial images from posterior to anterior are shown. See Key to Abbreviations on page 86.

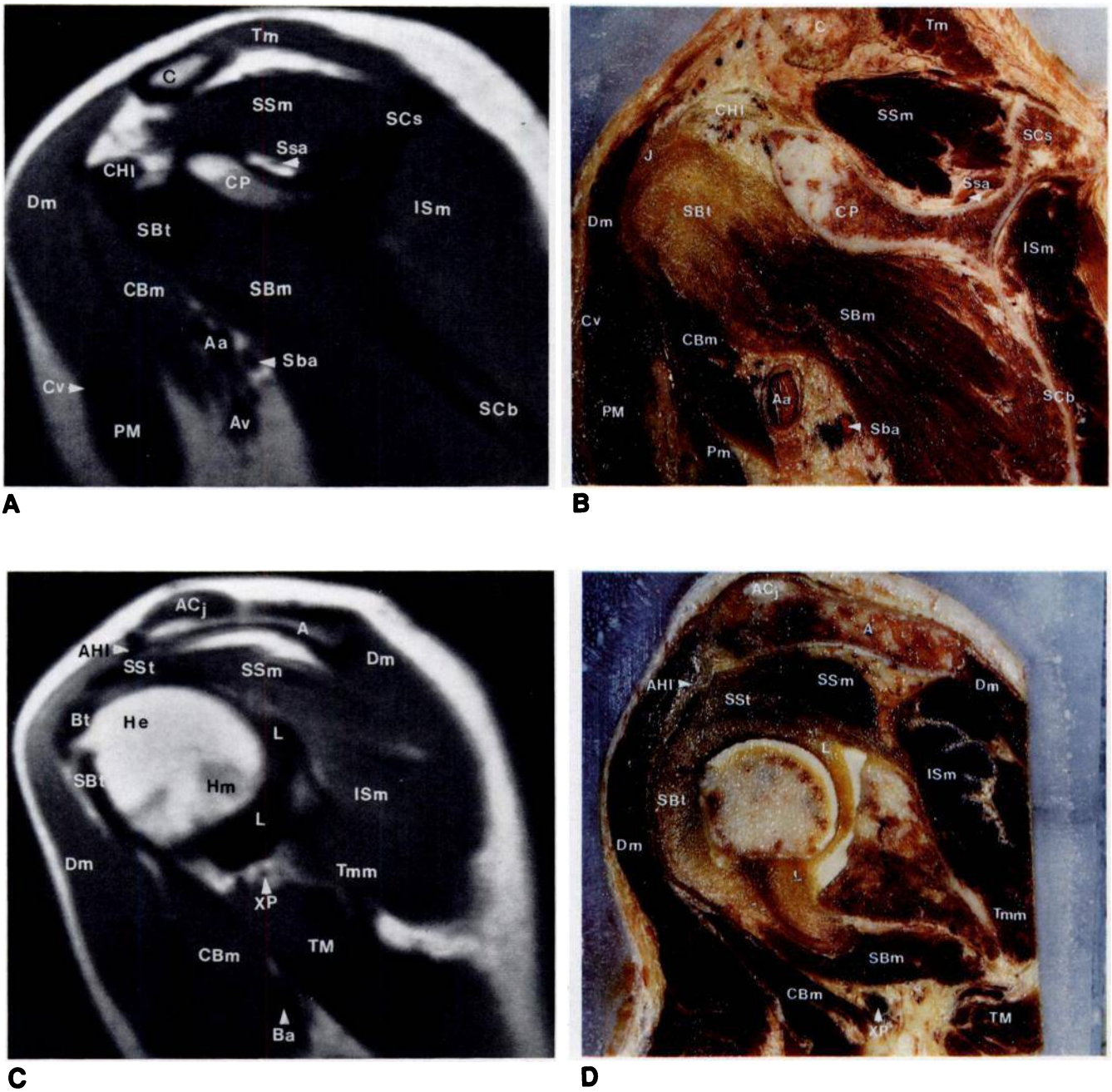

Fig. 4.—*A–H*, MR images and photographs of cadaver specimens made in the sagittal plane. Serial images from medial to lateral are shown. See Key to Abbreviations on page 86.

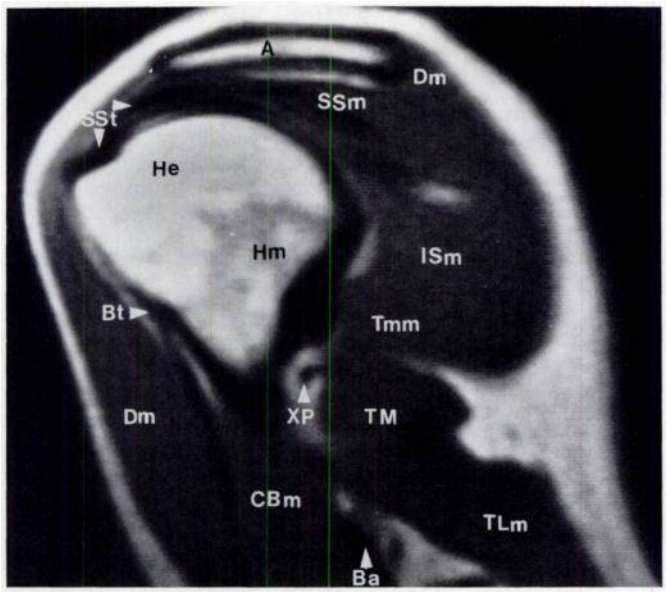

E

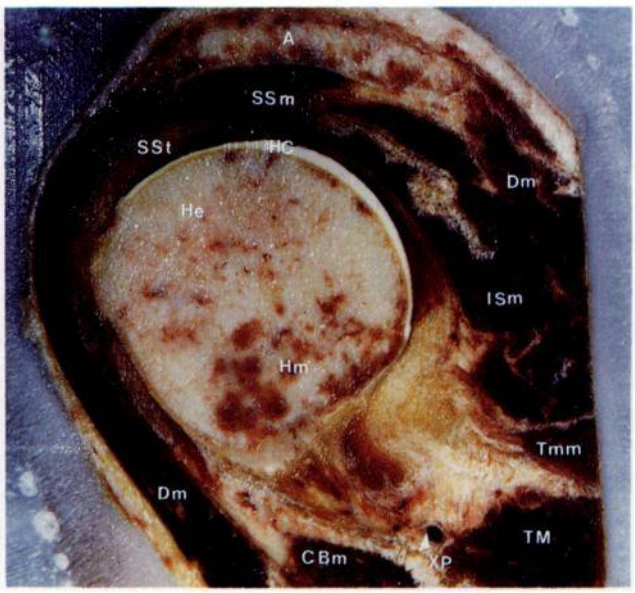

F

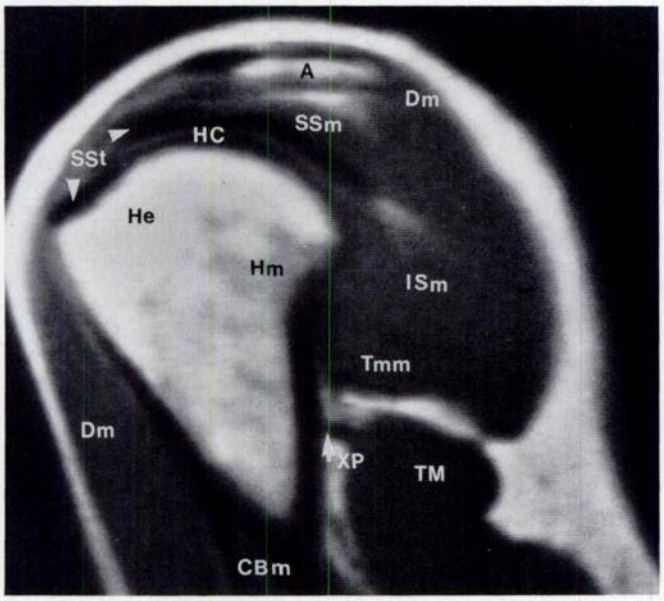

G

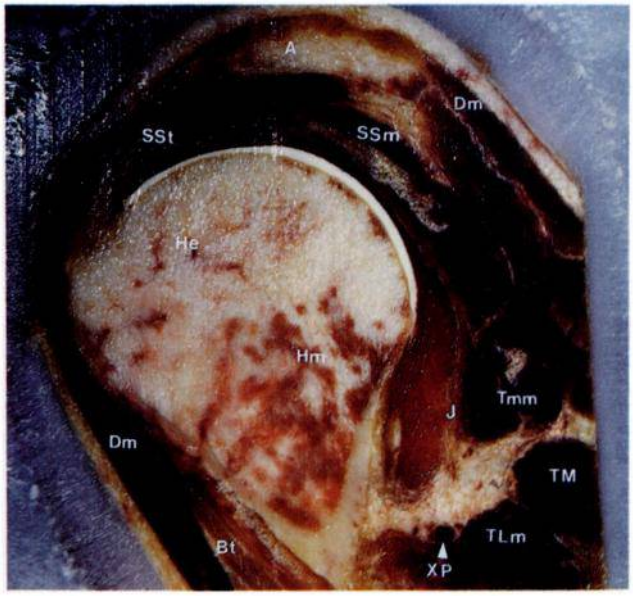

H

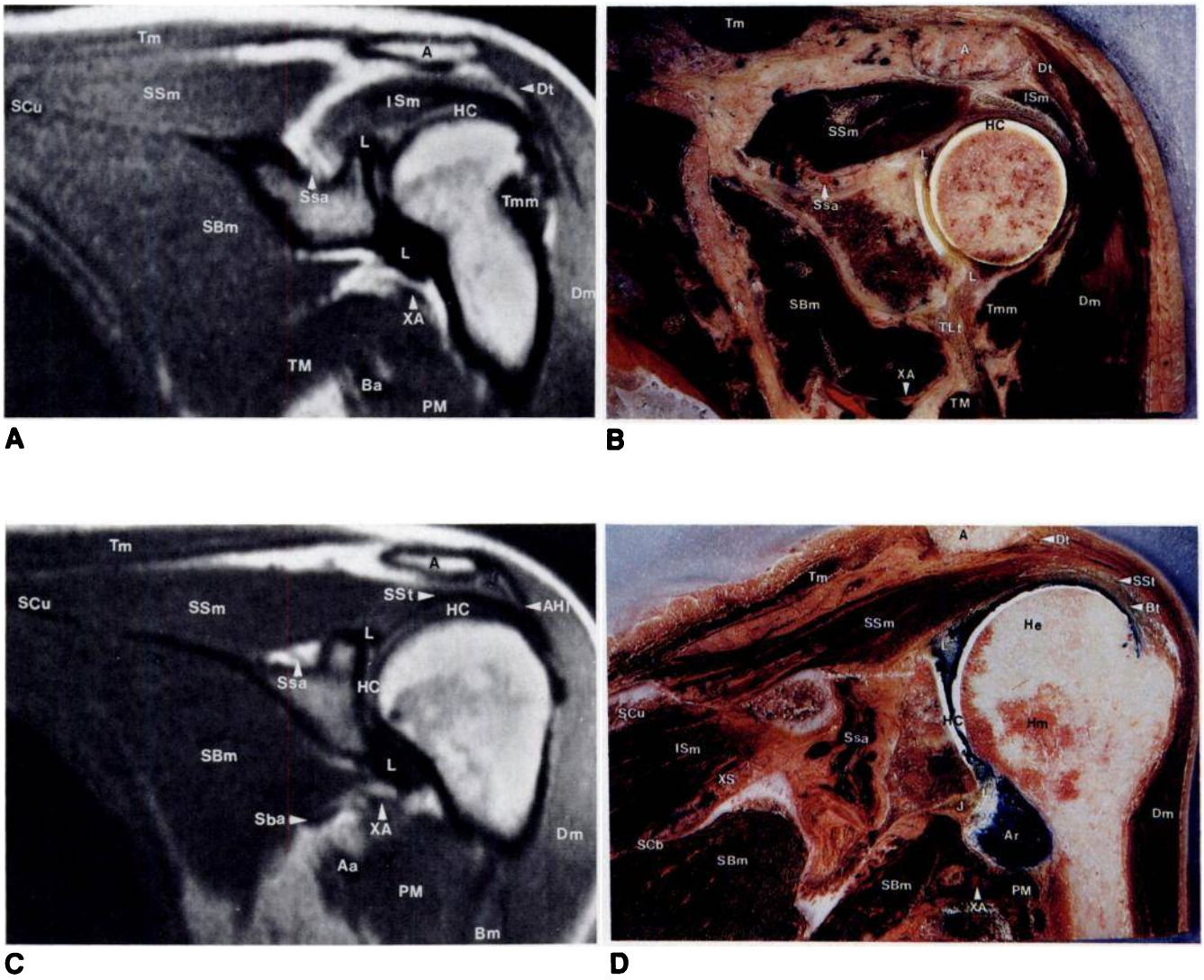

Fig. 5.—*A–H*, MR images and photographs of cadaver specimens made in the oblique plane. Serial images from posterior to anterior are shown. See Key to Abbreviations on page 86.

don is also evident. Because the coronal-to-sagittal angulation of the scapula is usually similar to the course of the supraspinatus muscle [11], this orientation is superior to the coronal plane for imaging the superior and larger inferior glenoid labra. The articular cartilage and coracoclavicular ligament are well seen.

ACKNOWLEDGMENTS

We thank the following people for their assistance with this project: John Robert (cadaver preparation), Val Gausche and Bobby Keen (technical assistance with scanning), Jerry Spellman (technical advice for development of scanning technique), and Jan Votruba, James Genova, and Neil Schaknowski (surface-coil development and production).

REFERENCES

1. Daffner RH, Lupetin AR, Dash N, Deeb ZL, Sefczek RJ, Schapiro RL. MRI in the detection of malignant infiltration of bone marrow. *AJR* **1986**;146:353–358
2. Aisen AM, Martel W, Braunstein EM, McMillin KI, Phillips WA, Kling TF. MRI and CT evaluation of primary bone and soft-tissue tumors. *AJR* **1986**;146:749–756
3. Moon KL, Genant HK, Davis PL, et al. Nuclear magnetic resonance imaging in orthopaedics: principles and applications. *J Orthop Res* **1983**;1:101–114
4. Li KC, Henkelman RM, Poon PY, Rubenstein J. MR imaging of the normal knee. *J Comput Assist Tomogr* **1984**;8:1147–1154
5. Fisher MR, Barker B, Amparo EG, et al. MR imaging using specialized coils. *Radiology* **1985**;157:443–447
6. Ehman RL. MR imaging with surface coils. *Radiology* **1985**;157:549–550
7. Huber DJ, Mueller E, Heubes P. Oblique magnetic resonance imaging of normal structures. *AJR* **1985**;145:843–846
8. Edelman RR, Stark DD, Saini S, et al. Oblique planes of section in MR imaging. *Radiology* **1986**;159:807–810
9. Rauschning W. Computed tomography and cryomicrotomy of lumbar spine specimens: a new technique for multiplanar anatomic correlation. *Spine* **1983**;8:170–180

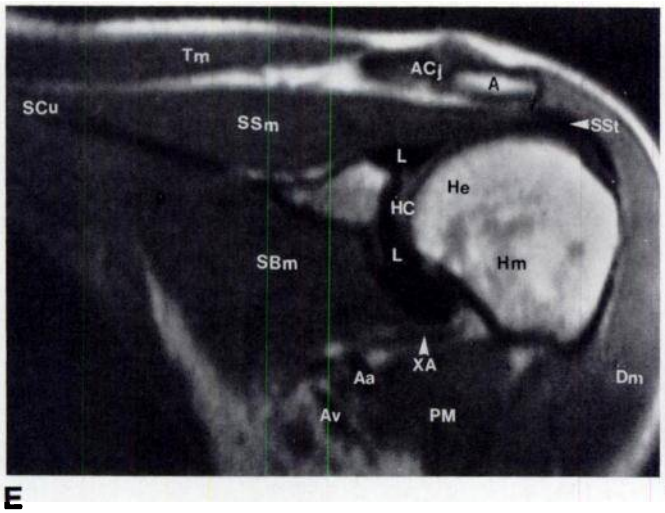

E

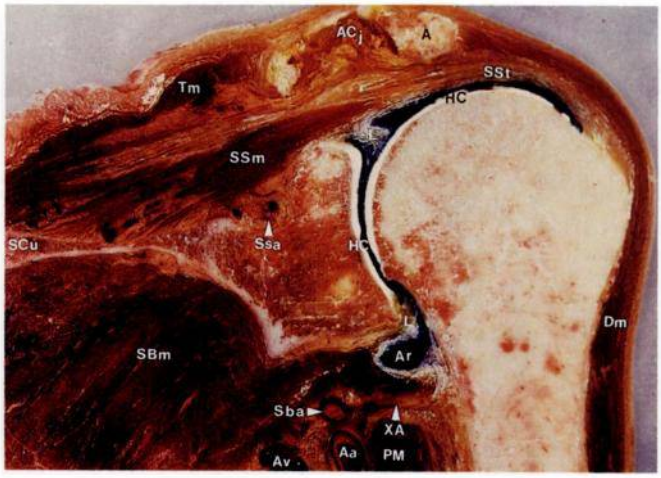

F

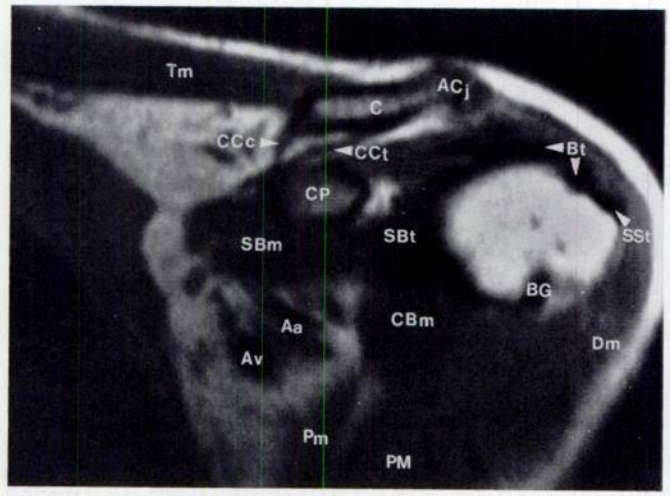

G

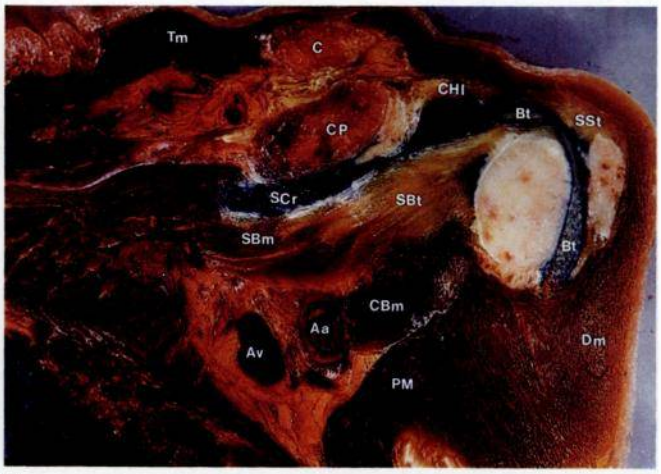

H

10. Moseley HF, Övergaard B. The anterior capsular mechanism in recurrent anterior dislocation of the shoulder: morphological and clinical studies with special reference to the glenoid labrum and the gleno-humeral ligaments. *J Bone Joint Surg [Br]* **1962**;44:913–927
11. Williams PL, Warwick R, eds. *Gray's anatomy*, 36th Br ed. Philadelphia: Saunders, **1980**:425–428, 489
12. Bateman JE. *The shoulder and environs.* St. Louis: Mosby, **1955**:62–63
13. Codman EA. *The shoulder: rupture of the supraspinatus tendon and other lesions in or about the subacromial bursa.* Malabar, FL: Kreiger, **1984**:22
14. Bloom W, Fawcett DW. *A textbook of histology*, 9th ed. Philadelphia: Saunders, **1968**:255–260
15. Boileau Grant JC. Interarticular synovial folds. *Br J Surg* **1931**;18:636–640

This article has been cited by:

1. Kenneth Sheah, Miriam A. BredellaShoulder 2159-2206. [CrossRef]
2. Kirk L. Jensen, Charles A. RockwoodRadiographic Evaluation of Shoulder Problems 177-212. [CrossRef]
3. Wayne Z. Burkhead, Peter Habermeyer, Gilles Walch, Kenneth LinThe Biceps Tendon 1309-1360. [CrossRef]
4. Nicholas G Mohtadi, A.Dale Vellet, Marcia L Clark, Robert M Hollinshead, Treny M Sasyniuk, Gordon H Fick, Phillip J Burton. 2004. A prospective, double-blind comparison of magnetic resonance imaging and arthroscopy in the evaluation of patients presenting with shoulder pain. *Journal of Shoulder and Elbow Surgery* **13**, 258-265. [CrossRef]
5. M P WILLIAMSON, V P CHANDNANI, D E BAIRD, T Q REEVES, T M DEBERARDINO, G W SWENSON, M F HANSEN. 1994. Shoulder impingement syndrome: Diagnostic accuracy of magnetic resonance imaging and radiographic signs. *Australasian Radiology* **38**, 265-271. [CrossRef]
6. Steven J. Hattrup, Robert H. Cofield, Thomas H. Berquist, Paul F. McGough, Pierre J. Hoffmeyer. 1992. Shoulder arthrography for determination of size of rotator cuff tear. *Journal of Shoulder and Elbow Surgery* **1**, 98-105. [CrossRef]
7. Vijay Chandnani, Charles Ho, Judith Gerharter, Christian Neumann, Sevil Kursunoglu-Brahme, David J. Sartoris, Donald Resnick. 1992. MR findings in asymptomatic shoulders: a blind analysis using symptomatic shoulders as controls. *Clinical Imaging* **16**, 25-30. [CrossRef]
8. Jeffrey Mace Boorstein, J.Bruce Kneeland, Murray Dalinka, Joseph P. Ianotti, Jin-Suck Suh. 1992. Magnetic resonance imaging of the shoulder. *Current Problems in Diagnostic Radiology* **21**, 5-27. [CrossRef]
9. Angela Jones, Iain Watt. 1989. Diagnostic imaging of the shoulder joint. *Baillière's Clinical Rheumatology* **3**, 475-510. [CrossRef]
10. R. Lufkin, W. Rauschning, L. Seeger, L. Bassett, W. Hanafee. 1987. Anatomic correlation of cadaver cryomicrotomy with magnetic resonance imaging. *Surgical and Radiologic Anatomy* **9**, 299-302. [CrossRef]